

FPMC2017-4225

ROBUST CONTROL LAW FOR PNEUMATIC ARTIFICIAL MUSCLES

Jonathon E. Slightam

Department of Mechanical Engineering
Marquette University
Milwaukee, WI 53233
Email: jonathon.slightam@mu.edu

Mark L. Nagurka

Department of Mechanical Engineering
Marquette University
Milwaukee, WI, 53233
mark.nagurka@mu.edu

ABSTRACT

This paper presents a modified integral sliding surface, sliding mode control law for pneumatic artificial muscles. The cutoff frequency tuning parameter λ is squared to increase the gradient from absement (integral of position) to position and higher derivatives to reflect the more dominant terms in the actuator dynamics. The sliding mode controller is coupled with proportional and integral action compensation. The control system is sufficiently robust so that use of an observer and input-output feedback linearization are not required. Closed-loop control experiments are compared with traditional sliding mode controller designs presented in the literature for pneumatic artificial muscles. Experiments include the tracking of sinusoidal waves at 0.5 and 1 Hz, tracking of square-like waves with seventh-order trajectory transitions at a rate of 0.2 Hz without and with a steady-state period of 10 seconds, as well as a step input response. These experiments indicate that the control law provides similar bandwidth, tracking, and steady-state performance as approaches requiring nonlinear feedback and model observation for pneumatic artificial muscles. Experiments demonstrate an accuracy of 50 μm at steady-state with no overshoot and maximum tracking errors less than 0.4 mm for smooth square-like trajectories.

INTRODUCTION

A pneumatic artificial muscle (PAM) is a type of flexible fluidic actuator (FFA) that contracts when pressurized with a working fluid. FFAs transmit mechanical power through large deformations of elastic or hyperelastic membranes by an energized fluid. They can be built in pro-

late (contractile), oblate (expansion), and helical (twisting) forms allowing for different modes of translation, rotation, and bending. A PAM consists of a rubber-like tube encapsulated by a fiber braid that has two end caps and contains the pressurized fluid. One of the end caps allows for a compressed gas (typically air) to flow in and out of the PAM.

Research on PAMs has focused on both nonlinear modeling and control. A significant body of the research suggests that nonlinear control approaches can achieve performance that is not possible with classical control methods. This paper presents a new sliding mode control (SMC) approach. It proposes using a squared tuning parameter λ in an integral sliding surface in a sliding mode position control law.

BACKGROUND

The first patent on PAMs dates back to 1929 [1]. A steady interest in PAMs emerged starting in the 1950s, mostly in the form of patents [2], [3], [4], [5]. Commercialization of PAMs was realized by Bridgestone and Dynacyle with additional patents awarded [6], [7], [8].

The background below provides a concise review of control approaches used for PAMs including linear control theory (classical and modern methods) and nonlinear control theory. This review gives insights to deficiencies that motivate the control method proposed in this paper.

Control Approaches for PAMs

Early control approaches for PAMs used experimental methods to implement position control. Paynter *et al.* modeled PAMs, called tuggers, by describing their change in enthalpy. Paynter used experimental correlations to implement open-loop position control [9], [10]. This approach was used for applications including vehicle suspension and engine mount vibration dampening [11].

Caldwell *et al.* were among one of the first to demonstrate closed-loop control of PAMs with discrete linear control theory [12]. In their early work, overshoot of 12% was shown in experiments and performance was highly sensitive to noise, changes in supply pressure, temperature, and tube length [12]. Surdilovic *et al.* demonstrated trajectory tracking of a PAM robot manipulator with an accuracy of 10 mm using linear control theory [13]. Situm *et al.* used a proportional-integral position controller for an antagonistic pair of PAMs, with a steady-state error of 18% from the set point value [14]. The data were presented as relative percent errors due to the output signal given as the raw voltage signal in [12] and [14].

Nonlinear control approaches have shown to improve motion control performance over classical and modern control methods for PAMs [15]. Sliding mode control is one such method, and there is a significant interest this approach within the fluid power motion control research community. SMC approaches are desirable due to their mathematical convergence of the error dynamics to zero over a given trajectory and ability to compensate for unmodeled dynamics and physical uncertainties [16].

De Volder *et al.* illustrated positioning accuracy of $\pm 30 \mu\text{m}$ using proportional integral SMC (PISMC) [17]. Shen *et al.* implemented a sliding mode control law on a chemically powered translating pair of antagonistic PAMs [18]. Shen reported tracking errors for sinusoidal trajectories at 0.5 and 1 Hz to be at a maximum 0.75 mm and 1.5 mm, respectively [18]. Lilly *et al.* reported SMC maximum tracking errors of an angular antagonistic pair of PAMs to be 1.15 degrees with a 20 kg payload [19]. Hirano *et al.* reported a maximum position tracking error of 1.17 mm for a PAM driven delta robot using a PI computed torque controller [20]. Sardellitti *et al.* reported torque and stiffness SMC for an antagonistic pair of PAMs, which resulted in maximum errors of 0.12 N-m and 0.06 N-m/rad for torque and stiffness, respectively [21]. Driver *et al.* reported a maximum tracking error of 3 degrees when tracking a 20 degree amplitude sinusoid at 1 Hz [22].

Summary and Scope

SMC techniques have proven to be superior over classical and modern theory methods for pneumatic and

highly nonlinear motion control applications such as FFAs and PAMs [18], [21], [22], [23]. The 2015 *Multi-Annual Roadmap for Robotics in Europe* emphasized that one of the top scientific needs to realize human-robot interaction is model-based control of soft actuators [24]. *A Roadmap for US Robotics - From Internet to Robotics* also identified that merging the design of actuator, mechanisms, and control is necessary for next generation mechanisms and actuators in robotics [25].

This paper presents a reduced order dynamic model of a PAM. The PAM model is used to derive a proposed SMC law with proportional and integral action compensation. The controller is robust, obviating the need to use observers and input-output feedback linearization. Tracking experiments for sinusoidal trajectories, square-like seventh-order trajectories, and a step response are conducted and the maximum tracking errors and steady-state error are reported.

MODELING Actuator Dynamics

One configuration of a PAM is made of a rubber tube encompassed by a helical fiber braid with end caps as illustrated in Figure 1 (top). The length L of the PAM is

$$L = L_0 - x \quad (1)$$

where L_0 is the initial length of the PAM and x is the displacement of the free end of the PAM (positive displacement is towards the fixed end of the PAM). The length L is also related to the helical fiber length, b , of the braid that wraps around the rubber tube and angle of the fiber relative to the primary axis by $L = b \cos \theta$. The force from the PAM from increased internal pressure is a result of the reaction forces of the braid and rubber tube acting on the end caps. The free-body diagram is shown in Figure 1 (bottom). The forces acting on the PAM can be derived using the principle of virtual work as developed by Gaylord [26] and then Chao and Hannaford, [27], $F = -P(dV/dL)$. Since the control volume is a function of actuator length, L , the volume of the PAM is

$$V = L(b^2 - L^2)/(4\pi n^2) \quad (2)$$

and the force produced by the actuator from the internal pressure then becomes

$$F = \frac{P(3L^2 - b^2)}{4\pi n^2} \quad (3)$$

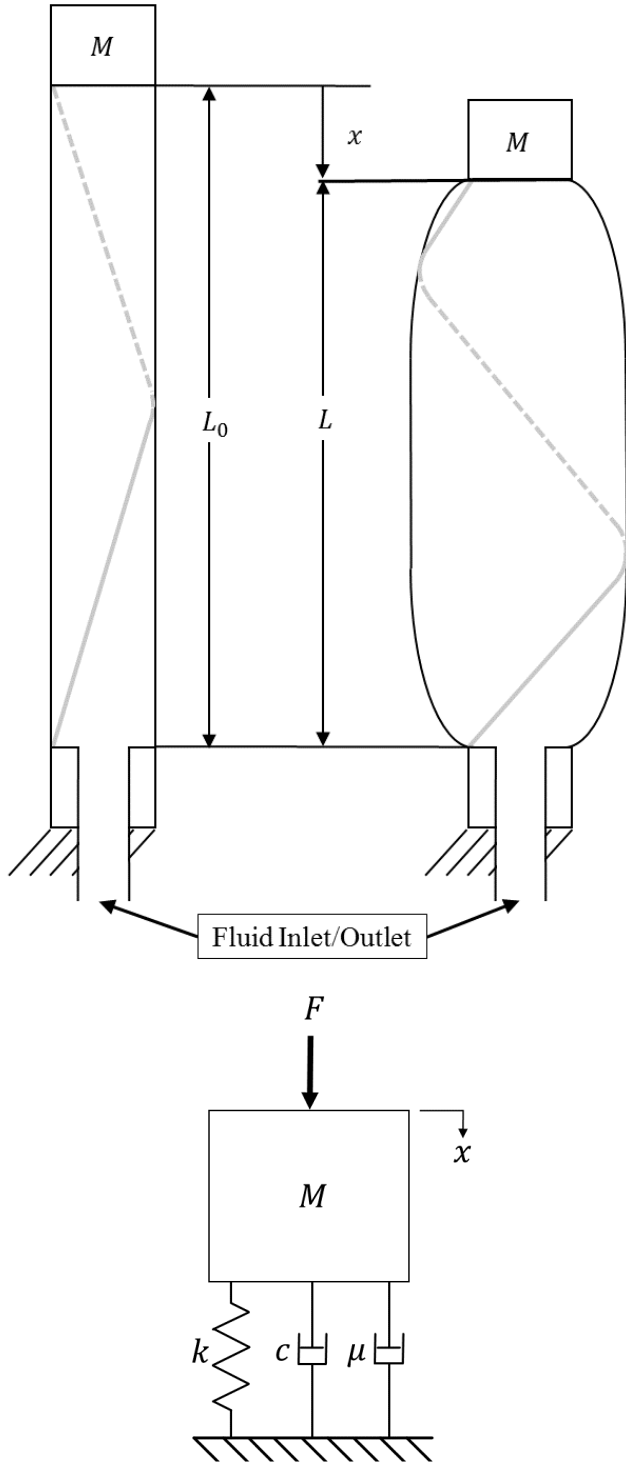


FIGURE 1. PNEUMATIC ARTIFICIAL MUSCLE DIAGRAM AND FREE-BODY DIAGRAM OF MODEL.

In equations 2 and 3, n is the number of turns the fiber braid wraps around the tube. This force represents the input to the equation of motion from Newton's second law,

$$M\ddot{x} + c\dot{x} + \mu\dot{x}P + kx = \frac{P(3L^2 - b^2)}{4\pi n^2} \quad (4)$$

where k is the stiffness of the actuator material, internal pressure, and change in geometry, c is the viscous damping coefficient, μ is the area normalized coefficient of friction between the fiber braid and the hyperelastic tube, and M is the mass of the non-fixed end of the PAM. The actuator stiffness, k , is assumed to be linear. Some models present Mooney-Rivlin approaches that could be implemented, but are computationally intensive [28].

In state-space form, Equation 4 can be expressed as

$$\begin{pmatrix} \dot{x}_1 \\ \dot{x}_2 \end{pmatrix} = \begin{pmatrix} x_2 \\ \frac{1}{M} \left(\frac{P(3(L_0 - x_1)^2 - b^2)}{4\pi n^2} - c\dot{x}_1 - \mu\dot{x}P - kx_1 \right) \end{pmatrix} \quad (5)$$

The actuator model parameters are listed in Table 1.

TABLE 1. ACTUATOR PARAMETERS.

Parameter	Value	Parameter	Value
M	0.45 kg	L_0	203.2 mm
c	1.31 N-s/mm	b	22.5 mm
n	1	k	254 N/mm
μ	15.1 mm-s	D	20 mm

Pressure Dynamics

The pressure dynamics for the PAM are modeled for the actuator control volume (the internal volume of the actuator shown in Figure 1) and a proportional flow control valve. The pressure rate of change of the PAM control volume is the time derivative of the ideal gas law, giving

$$\dot{P} = \frac{RT}{V}\dot{m} - \frac{P}{V}\dot{V} \quad (6)$$

where R is the universal gas constant for air, T is the absolute temperature of the air, V is the volume of the actuator, \dot{V} is the rate of change of volume, and \dot{m} is the mass flow rate. The pressure dynamics are assumed to be isothermal

and the mathematical models are explained in more detail in [29], [23], [30] and [31]. The mass flow rate is modeled as isentropic flow through a plate with a small hole (aperture). The mass flow rate is a function of the aperture cross-sectional area of the spool valve, and the area normalized flow rate, Ψ , as described by

$$\dot{m} = A_v \Psi \quad (7)$$

where the aperture area A_v is assumed to be linearly proportional to the spool position, that is proportional to the command signal, u , discussed later. The area normalized mass flow rate is a piecewise function governed by choked and unchoked flow regimes that is based on the quotient of the downstream and upstream pressures, respectively,

$$\Psi(P_u, P_d) = \begin{cases} \Psi_c & \frac{P_d}{P_u} \leq C_r \text{ Choked} \\ \Psi_{uc} & \frac{P_d}{P_u} > C_r \text{ Unchoked} \end{cases} \quad (8)$$

where Ψ_c is the choked area normalized mass flow rate defined by,

$$\Psi_c = \frac{C_1 C_f P_u}{\sqrt{T}} \quad (9)$$

and Ψ_{uc} is the unchoked area normalized mass flow defined by,

$$\Psi_{uc} = \frac{C_2 C_f P_u}{\sqrt{T}} \left(\frac{P_d}{P_u} \right)^{1/\gamma} \sqrt{1 - \left(\frac{P_d}{P_u} \right)^{(\gamma-1)/\gamma}} \quad (10)$$

The coefficients C_1 and C_2 are gas properties, C_f is a nondimensional discharge coefficient, γ is the ratio of specific heats, and C_r is the threshold between choked and unchoked flow through the valve. For air, C_r is 0.528, C_f is 0.2939, and C_1 and C_2 are

$$C_1 = \sqrt{\left(\frac{2\gamma}{R(\gamma+1)} \right)^{\frac{\gamma+1}{\gamma-1}}} \quad (11)$$

and

$$C_2 = \sqrt{\frac{2\gamma}{R(\gamma-1)}} \quad (12)$$

For the internal chamber and proportional valve used, Ψ is governed by

$$\Psi(P_1, P_s, P_{atm}) = \begin{cases} P_d = P_1, P_u = P_{source} & A_v \geq 0 \\ P_d = P_{atm}, P_u = P_1 & A_v < 0 \end{cases} \quad (13)$$

where P_d is the downstream pressure, P_1 is the actuator internal pressure, P_u is the upstream pressure, P_{atm} is the atmospheric pressure, and P_{source} or P_s is the source pressure. The volume inside the actuator as a function of length is described in Equation 2 and the time rate of change in volume is

$$\dot{V} = \frac{b^2 - 3L^2}{4\pi n^2} \dot{L} \quad (14)$$

In state-space form, the pressure dynamics of the PAM are

$$\dot{p} = \dot{x}_3 = \frac{RT\Psi K_{av}}{V(x_1)} u - \frac{x_3 \dot{V}(x_1, x_2)}{V(x_1)} \quad (15)$$

where K_{av} is the proportional gain relating the input voltage and aperture area $A_v = K_{av}u$, with $K_{av} = 2mm^2/V$. The input command voltage is ± 2.5 V. The pneumatic system properties are listed in Table 2.

TABLE 2. PNEUMATIC SYSTEM PARAMETERS.

Parameter	Value	Parameter	Value
P_{source}	441.3 kPa	A_v	$\pm 5.000 \text{ mm}^2$
P_{atm}	101.3 kPa	C_d	0.5898
R	287.1 J kg ⁻¹ K ⁻¹	C_f	0.2800
C_1	0.04040	T	273.0 K
C_2	1.156	γ	1.400

System Dynamics

The system model in state-space form can be constructed by combining Equations 5 and 15, giving

$$\begin{pmatrix} \dot{x}_1 \\ \dot{x}_2 \\ \dot{x}_3 \end{pmatrix} = \begin{pmatrix} x_2 \\ \frac{1}{M} \left(\frac{x_3(3(L_0-x_1)^2-b^2)}{4\pi n^2} - c\dot{x}_1 - \mu\dot{x}_3 - kx_1 \right) \\ \frac{RT\Psi K_{av}}{V(x_1)} u - \frac{x_3 \dot{V}(x_1, x_2)}{V(x_1)} \end{pmatrix} \quad (16)$$

Research suggests that a third-order lumped parameter model can predict the dynamic behavior of a PAM [32]. However, valves that are not high performance or long pneumatic lines can make this third-order model insufficient. Knowing the order of the model that accurately describes the system and the desired state trajectory being controlled, a robust nonlinear control law can be derived, such as presented by Slotine for a traditional sliding surface, $s = (d/dt + \lambda)^{m-1} e$ and an integral sliding surface $s = (d/dt + \lambda)^m \int e$ [16].

SLIDING MODE POSITION CONTROL

Traditional SMC approaches for PAMs use an integral sliding surface, resulting in a 3rd-order sliding surface for the 3rd-order position tracking control problems. An integral sliding surface takes on the form $s = (\frac{d}{dt} + \lambda)^m \int e$ where m is the order of the differential equations describing the system to be controlled [16], [23]. Due to a majority of the nonlinearities from the actuator mechanics, it is proposed that the sliding surface is weighted more so on the lower order terms in s . To do this, the constant λ is squared to increase the gradient from absent (integral of position) to position and higher order terms [33].

$$s = \left(\frac{d}{dt} + \lambda^2 \right)^m \int e \quad (17)$$

Expanding Equation 17 for a third-order system results in the sliding surface:

$$s = \ddot{e} + 3\lambda^2 \dot{e} + 3\lambda^4 e + \lambda^6 \int e \quad (18)$$

Differentiating Equation 18 with respect to time

$$\dot{s} = \ddot{\ddot{e}} + 3\lambda^2 \ddot{e} + 3\lambda^4 \dot{e} + \lambda^6 e \quad (19)$$

The equivalent control law can be expressed using Filippov's equivalent dynamics principle

$$u_{eq} = \frac{1}{\hat{g}} \left(\ddot{x}_D + \hat{f} - 3\lambda^2 \ddot{e} - 3\lambda^4 \dot{e} - \lambda^6 e \right) \quad (20)$$

where \hat{f} and \hat{g} are model estimation parameters determined by solving for control input in the third order model, similar to those presented in [23] and [32]. With a

Lyapunov like function, $\frac{1}{2} \frac{d}{dt} s^2 \leq -\eta |s|$, the robust control law is determined to be

$$u_{rb} = \eta |s| \operatorname{sgn}(s) \quad (21)$$

to keep the scalar s , the sliding surface, at zero. The sgn is a sign function for s where $\operatorname{sgn}(s) = +1$ if $s > 0$ and $\operatorname{sgn}(s) = -1$ if $s < 0$. To eliminate any chatter from the high speed switching, a saturation function using the variable ϕ is introduced to act as a first-order filter, with the saturation of s/ϕ being at ± 1 .

$$u_{rb} = \eta |s| \operatorname{sat} \left(\frac{s}{\phi} \right) \quad (22)$$

Combining the equivalent and robust control laws results in the 3rd-order, quadratic integral sliding surface, sliding mode position control law:

$$u = \frac{1}{\hat{g}} \left(\ddot{x}_D + \hat{f} - 3\lambda^2 \ddot{e} - 3\lambda^4 \dot{e} - \lambda^6 \eta |s| \operatorname{sat} \left(\frac{s}{\phi} \right) \right) \quad (23)$$

Here we make the assumption that the control law is sufficiently robust such that an observer and input-output feedback linearization are not needed. Thus, the SMC becomes

$$u_{SMC} = \ddot{x}_D - 3\lambda^2 \ddot{e} - 3\lambda^4 \dot{e} - \lambda^6 \eta |s| \operatorname{sat} \left(\frac{s}{\phi} \right) \quad (24)$$

Adding proportional and integral action results in a PISMC law for the PAM,

$$u_{PIDSMC} = u_{SMC} \left(K_p + K_i \int dt \right) \quad (25)$$

The PISMC tuning parameters determined empirically are listed in Table 3. The PISMC was tuned by first adjusting the parameter λ , followed by incrementally increasing η to achieve the desired track while simultaneously increasing ϕ to eliminate chatter. The PI compensator gains were then adjusted to further improve the response and steady-state performance.

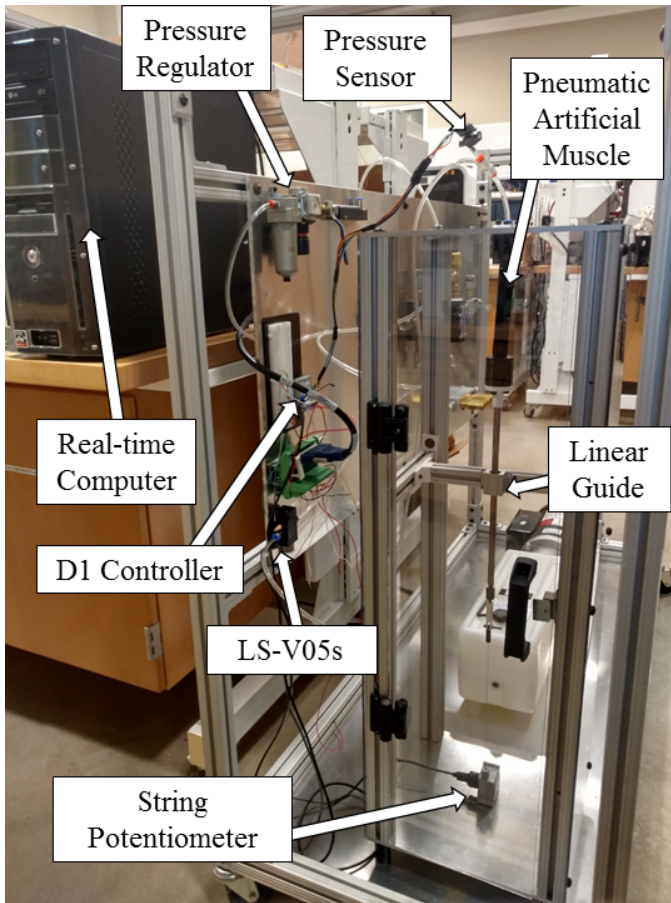
A first-order low pass filter ($FO - LPF_{co}$) was used to filter the measured position signal x into the PISMC; otherwise, significant signal noise would be amplified by the numerical differentiation in the control law.

TABLE 3. SMC PARAMETERS.

Parameter	Value	Parameter	Value
$FO - LPF_{co}$	100 Hz	λ	10 Hz
ϕ	25 mm/s ²	η	0.05 mm/s ³
K_p	1.3	K_i	0.125

EXPERIMENTAL SETUP

A test fixture was designed and built for conducting control experiments with artificial muscles as shown in Figure 2. The PAM is controlled and tested via Simulink

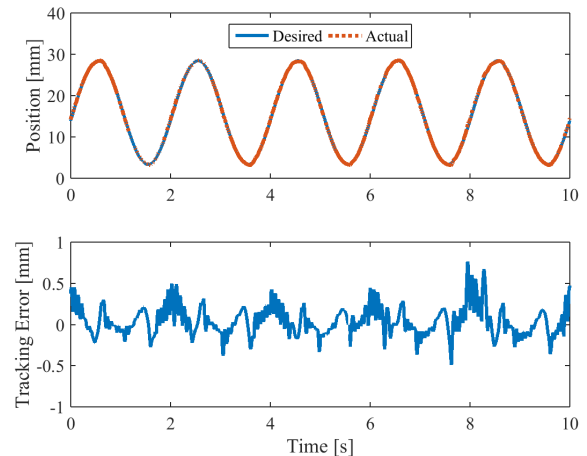
**FIGURE 2.** EXPERIMENTAL SETUP.

Real-time with a desktop computer using a National Instruments PCI-6221 Multipurpose data acquisition card (with 32 pin connector). An Enfield Technologies LS-V05s proportional pneumatic control valve is used that has a bandwidth of 109 Hz and exhibits low hysteresis. A voltage command signal is sent from the data acquisition card

to an Enfield Technologies D1 proportional linear motor valve driver. The proportional flow control valve controls the mass flow rate from the pneumatic pressure source at the manifold to the PAM or from the PAM exhausted to atmosphere. Between the valve and the PAM, a NPX MPX5700GP pressure sensor is used to record the pressure dynamics. The PAM is connected to a SP2-12 string potentiometer from Measurement Specialties.

RESULTS

Five different tracking experiments were conducted. The controller was tested following a sinusoidal trajectory of 1 and 0.5 Hz with an amplitude of 12.7 mm and an offset of 15.88 mm, as well as a square-like seventh-order polynomial trajectory with an amplitude of 12.7 mm and an offset of 15.88 mm, at 0.2 Hz transitions between set points, with no steady state period and a resting period of 0.1 Hz. Figures 3 and 4 show the tracking of a sinusoidal wave at 0.5 and 1 Hz, respectively.

**FIGURE 3.** SINUSOIDAL TRACKING AT 0.5 Hz.

The tracking experiment of the sinusoidal wave at 0.5 Hz showed a maximum tracking error of approximately 0.71 mm just past the inflection points of the sine wave when retracting towards its original length L_0 . Tracking of the sinusoidal wave at 1 Hz illustrated a maximum tracking error of approximately 1.9 mm at the same locations.

Figures 5 and 6 show the tracking of a continuous square-like wave with seventh-order polynomial transitions at a frequency of 0.2 Hz, without and with a resting period of 10 s, respectively.

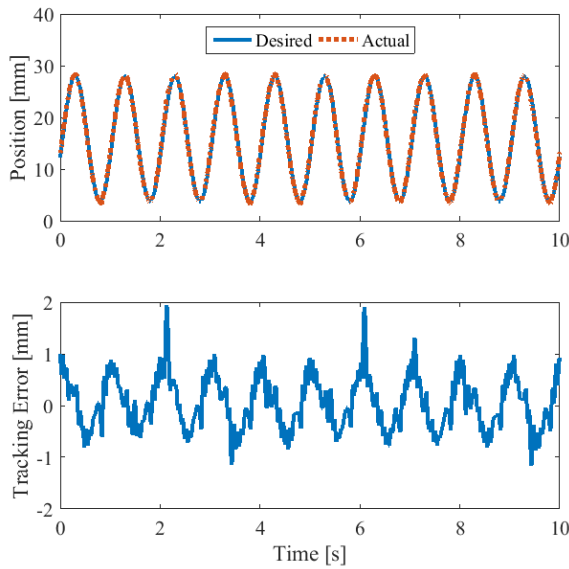


FIGURE 4. SINUSOIDAL TRACKING AT 1 HZ.

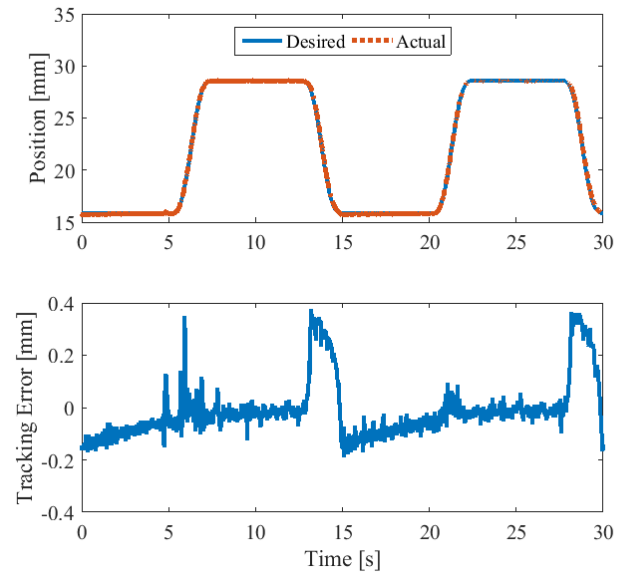


FIGURE 6. SEVENTH-ORDER TRAJECTORY WITH 0.1 HZ REST PERIOD TRACKING.

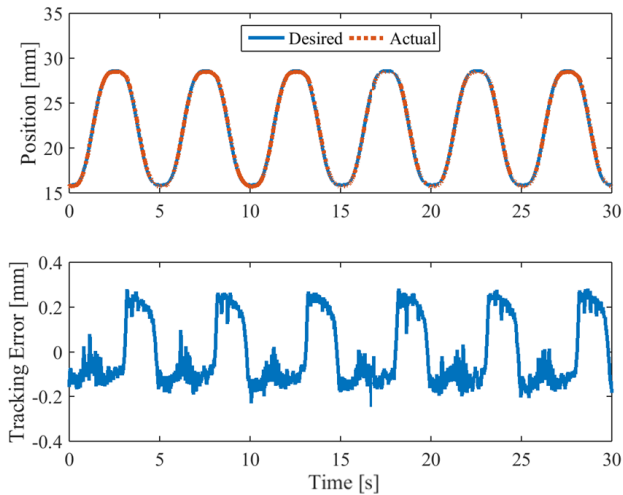


FIGURE 5. SEVENTH-ORDER TRAJECTORY TRACKING.

Both seventh-order trajectory tracking experiments exhibited tracking errors of 0.38 mm or less. These two experiments also show improved tracking characteristics for the PAM being pressurized as opposed to depressurized. For the seventh-order trajectory tracking experiment with a 10 s resting period the approximate steady-state accuracy of the controller was approximately $50 \mu\text{m}$.

The step response of the PISMIC for the PAM illustrates no overshoot yet the actuator achieves sub $100 \mu\text{m}$ accuracy in less than 0.5 s. After 5 s, $50 \mu\text{m}$ accuracy is achieved.

From the phase plane trajectory of the step response this controller does not follow the typical slope of $-\lambda$ when in the sliding mode, as shown in Figure 8.

The maximum tracking and steady-state (S.S.) errors are listed in Table 4.

TABLE 4. CONTROLLER PERFORMANCE.

Trajectory	Max. Error [mm]	S.S. Error [mm]
Sine (0.5 Hz)	0.71	–
Sine (1.0 Hz)	1.9	–
7th-Ord.	0.37	–
7th-Ord. w/ Rest	0.38	0.05
Step	–	0.05

DISCUSSION

The results of the modified sliding surface PISMIC demonstrate a positioning accuracy of approximately $50 \mu\text{m}$, or $20 \mu\text{m}$ greater than the accuracy reported by De Volder *et al.* [17]. The maximum tracking errors for sinusoidal waves are less than those reported in the literature [18], [19]. The controller also shows similar response and tracking performance compared to SMCs implemented for

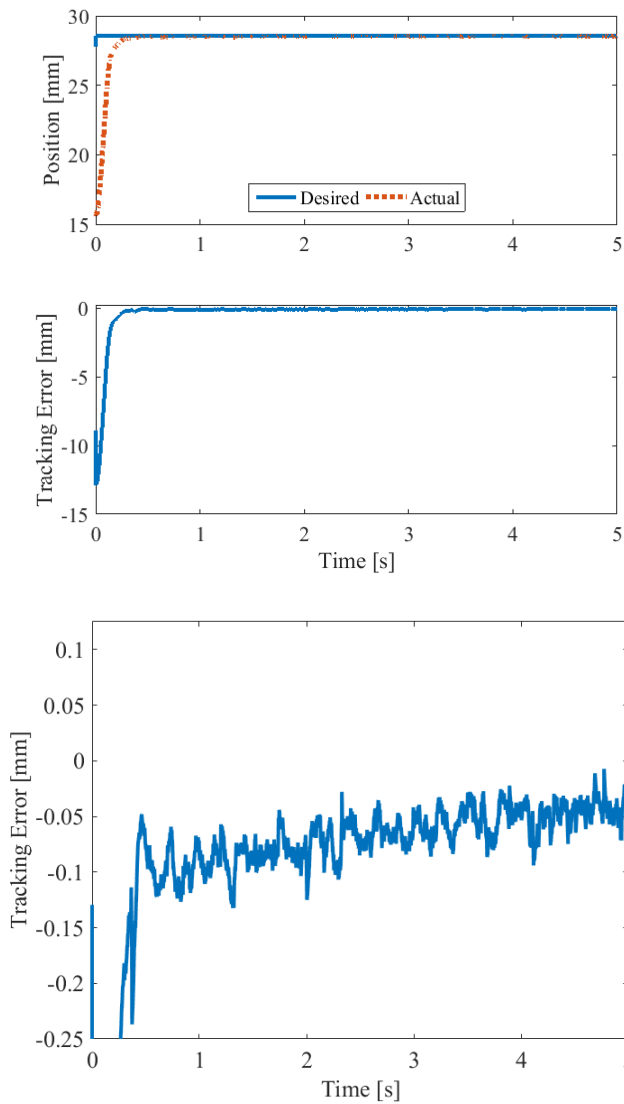


FIGURE 7. STEP RESPONSE AND ZOOMED ERROR.

PAMs that utilize model observation [22], [18], [17], [19], [15].

Maintaining the performance while eliminating the need for observers in SMCs may allow for more widespread use of this control approach. Since this method is computationally less expensive than traditional SMC approaches, it may be useful in the implementation of more complex multi-degree-of-freedom systems, as typical robot joints using PAMs rely on antagonistic pairs. As a result, more applications and utilization of PAMs and other similar FFA devices in robots may be realized.

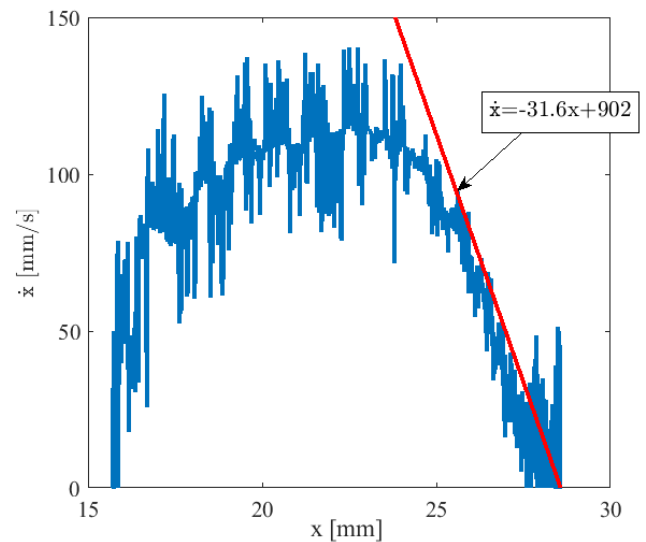


FIGURE 8. FINITE REACHING AND SLIDING MODE OF STEP RESPONSE.

CONCLUSIONS

This paper presented a modified sliding surface for a PISM. The sliding surface order was determined from acceptable lumped parameter models that can describe the dynamic behavior of the PAM. For the five control experiments conducted, the maximum tracking error was 1.9 mm in tracking a sinusoidal wave of 1 Hz, 0.38 mm while tracking a seventh-order square-like wave, a step response position accuracy of less than 0.1 mm in under 0.5 s with no overshoot, and a steady-state position accuracy of 50 μm . The proposed control law gives position control performance similar to traditional SMC methods for PAMs, without needing an observer and input-output feedback linearization.

REFERENCES

- [1] Lavaud, D. S. D., 1929. "Apparatus for generating an over-or-under pressure in gases or liquids". *Patent DE503775C, Germany*.
- [2] Henri, M. A., 1953. "Elastic diaphragm". *US Patent 2642091*.
- [3] Woods, J., 1957. Mechanical Transducer with Expandable Cavity. U.S. Patent 2789580.
- [4] Gaylord, R., 1957. "Fluid actuated motor system and stroking device". *US Patent 2844126*.
- [5] Barber, L., and Nickle, V., 1969. "Carbon Dioxide-Powered Arm and Hand Devices". *The American Journal of Occupational Therapy*, 23(3), p. 215.
- [6] Paynter, H., and Dynacycle Corp., 1974. Tension Ac-

- tuated Pressurized Gas Driven Rotary Motors. U.S. Patent 3854383.
- [7] Paynter, H., 1978. Fluid-Driven Torsional Operators for Turning Rotary Valves and the like. U.S. Patent 4108050.
- [8] Takagi, T., Sakaguchi, Y., and Bridgestone Corp., 1984. Pneumatic Actuator for Manipulator. Patent EP0123558 A2.
- [9] Paynter, H., and Jaurez, J., 2000. "Thermodynamic Analysis of Mechatronic Pneumatic Driven Spherical Joint". *IEEE/ASME Transactions on Mechatronics*, 5(2).
- [10] Paynter, H., 1996. "Thermodynamic Treatment of Tug-n-Twist Technology: Part 1. Thermodynamic Tugger Design". *Japan/USA Symposium on Flexible Automation*, 1, pp. 111–117.
- [11] Paynter, H., and Nagurka, M., 1997. "Hybrid Tension-Compression Pneumatic Actuators for Active Leveling, Tuning, and Damping of Vehicle Suspensions and Engine Mounts". *Proceedings of the 1997 IEEE Conference on Control Applications*, p. 630.
- [12] Caldwell, D. G., Medrano-Cerda, G. A., and Goodwin, M. J., 1993. "Braided Pneumatic Actuator Control of a Multi-Jointed Manipulator". *Proceedings of the 1993 IEEE Conference on Systems, Man, and Cybernetics*, Oct. 17-20, pp. 423–428.
- [13] Surdivolic, D., Radojicic, J., Schulze, M., and Dembek, M., 2008. "Modular Hybrid Robots with Biologically Inspired Actuators and Joint Stiffness Control". *Proceedings of the 2nd Biennial IEEE/RAS-EMBS International Conference on Biomedical Robotics and Biomechanics*, Oct. 19-22, pp. 289–294.
- [14] Situm, Z., and Herceg, S., 2008. "Design and Control of a Manipulator Arm Driven by Pneumatic Muscle Actuators". *16th Mediterranean Conference on Control and Automation*, June 25-27, pp. 926–931.
- [15] Liu, H., Zhao, Y., Jiang, F., and Yao, X., 2015. "Pneumatic Muscle Actuator Position Control Based on Sliding Mode Control Algorithms". *Proceedings of the 2015 IEEE International Conference on Information and Automation*, Aug. 8-10, pp. 1115–1120.
- [16] Slotine, J., and Li, W., 1991. *Applied Nonlinear Control*. Prentice Hall.
- [17] Volder, M. D., Coosemans, J., Puers, R., and Reynaerts, D., 2008. "Characterization and Control of a Pneumatic Microactuator with Integrated Inductive Position Sensor". *Journal of Sensors and Actuators*, 141(1), pp. 192–200.
- [18] Shen, X., and Christ, D., 2011. "Design and Control of Chemomuscle: A Liquid-Propellant-Powered Muscle Actuation System". *ASME Journal of Dynamic Systems, Measurement, and Control*, 133(2).
- [19] Lilly, J., and Yang, L., 2005. "Sliding Mode Tracking for Pneumatic Muscle Actuators in Opposing Pair Configuration". *IEEE Transactions on Control Systems Technology*, 13(4), pp. 550–558.
- [20] Hirano, J., Tanaka, D., Watanabe, T., and Nakamura, T., 2014. "Development of Delta Robot Driven by Pneumatic Artificial Muscles". *2014 IEEE/ASME International Conference on Advanced Intelligent Mechatronics*, July 8-11, pp. 1400–1405.
- [21] Sardenillitti, I., Palli, G., Tsagarakis, N. G., and Caldwell, D. G., 2010. "Antagonistically Actuated Compliant Joint: Torque and Stiffness Control". *The 2010 IEEE/RSJ International Conference on Intelligent Robots and Systems*, Oct. 18-22, pp. 1909–1914.
- [22] Driver, T. A., and Shen, X., 2014. "Design and Control of a Sleeve Muscle-Actuated Robot Elbow". *ASME Journal of Dynamic Systems, Measurement, and Control*, 136(1).
- [23] Comber, D., Slightam, J., Gervasi, V., Webster III, R.J., and Barth, E., 2013. "Design and Precision Control of an MR-Compatible Flexible Fluidic Actuator". *Proc. ASME/Bath Symposium on Fluid Power and Motion Control*, pp. 1–9.
- [24] for Robotics In Europe, T. P., 2015. *Robotics 2020 Multi-Annual Roadmap for Robotics in Europe*. Tech. rep.
- [25] Robotics Virtual Organization, 2013. *A Roadmap for U.S. Robotics-From Internet to Robotics*. Tech. rep.
- [26] Gaylord, R., 1958. Fluid Actuated Motor System and Stroking Device. U.S. Patent 2844126.
- [27] Chou, C.-P., and Hannaford, B., 1996. "Measurement and Modeling of McKibben Pneumatic Artificial Muscles". *IEEE Transactions on Robotics and Automation*, 12(1).
- [28] Ball, E., and Garcia, E., 2016. "Effects of Bladder Geometry on Pneumatic Artificial Muscles". *ASME Journal of Medical Devices*, 10(1), December.
- [29] Comber, D., Barth, E., and III, R. W., 2014. "Design and Control of an MR-Compatible Precision Pneumatic Active Cannula Robot". *ASME J Medical Devices*, 8(1).
- [30] Zhu, Y., and Barth, E. J., 2010. "Accurate Sub-Millimeter Servo-Pneumatic Tracking Using Model Reference Adaptive Control (MRAC)". *International Journal of Fluid Power*, 11(2), pp. 49–57.
- [31] Richer, E., and Hurmuzlu, Y., 2000. "A High Performance Pneumatic Force Actuator System: Part 1 - Nonlinear Mathematical Model". *ASME Journal of Dynamic Systems, Measurement, and Control*, 122(3), pp. 416–425.
- [32] Slightam, J. E., and Nagurka, M. L., 2016. "PID Sliding Mode Control of Prolate Flexible Pneumatic Actuators". *Proceedings of the ASME 2016 International Dy-*

dynamic Systems and Control Conference, Oct. 12-14. Minneapolis, USA.

- [33] Janzen, R., and Mann, S., 2014. "Actergy as a Reflex Performance Metric: Integral Kinematics Applications". *2014 IEEE Games Media Entertainment (GEM)*, Oct. 22-24.